

N 70 35912

CR 110084

Final Report

"The Mechanics of Viscoelastic Fluids"

Principal Investigator: Bruce Caswell

NASA Grant NGL 40-002-053

The following report on work carried out by the principal investigator at Brown University, Providence, R. I. is in two parts. The first part is a summary of results, and the second part consists of two manuscripts reporting work carried out under the grant.

CASE FILE
COPY

SUMMARY

The main results obtained during the period of the grant deal with low Reynolds number flow past small solid particles. This work was initiated under grant NsG-705 at the University of California (Davis). Consequently the report entitled "The Effect of Finite Boundaries on the Motion of Particles in non-Newtonian Fluids," which was submitted as part of the final report for grant NsG-705 also acknowledges the support of NGL 40-002-053. Because of its length, and at the suggestion of a referee, the above report is being published in two parts in Chemical Engineering Science. The first part retains the title above and is now in the press. The second part is entitled "The Stability of Particle Motion Near a Wall in Newtonian and non-Newtonian Fluids" and should be in print in a few months. These two manuscripts have not been forwarded to NASA since together they do not differ in any way from the original report previously submitted.

Two additional manuscripts are being submitted as part of the final report. These are: "Precision Falling Sphere Viscometry" (with D. A. Cygan, Ph.D. candidate, NASA Trainee), submitted to the Transactions of the Society of Rheology; "Measurement of the Rotational Drag on a Sphere at Low, Finite Reynolds Number" (with B. Mena, Ph.D. candidate), submitted to the Journal of Fluid Mechanics. The results reported in these papers are summarized below.

I. Experiments with Translating Spheres

D. A. Cygan has developed techniques for measuring terminal velocities which are highly accurate and reproducible. These are discussed in the paper above. Terminal velocities of spheres falling in tubes filled with a polyisobutylene solution have been interpreted in terms of the analysis derived by the principal investigator in "The Effect of Finite Boundaries on the Motion of Particles in non-Newtonian Fluids." The pertinent equations are:

$$\frac{6\pi a U_{\infty}}{F} = \frac{1}{\mu_0} - \frac{\lambda}{\mu_0} \left(\frac{F}{6\pi a^2} \right)^2 + 0 \left(\frac{F}{6\pi a^2} \right)^4, \quad (1)$$

where U_{∞} is the terminal velocity of a sphere moving in an unbounded Rivlin-Ericksen fluid under the influence of a force F . The characteristic time λ is a linear combination of constants of the third order fluid. This formula is valid in the limit of slow flow, and suggests a method for extrapolating data to obtain the zero-shear viscosity μ_0 . Values of U_{∞} are computed from measured velocities U according to the formula

$$U = U_{\infty} - \frac{F}{6\pi\mu_0 R} W(a/R) + 0(F/R)^3, \quad (2)$$

where R is the tube radius, and $W(a/R)$ is a function derived from Faxin's formula for the Newtonian case (equation (9) of Cygan's paper).

It is important to note that each of these formulae was derived under the assumption that the stress is given by the Rivlin-Ericksen theory in the limit of slow flow. When the Rivlin-Ericksen theory is taken as the slow flow asymptote of the general theory of simple fluids it is tantamount to imposing smoothness on the constitutive functional in the neighborhood of the rest state. In particular, it implies that the viscosity function departs from μ_0 as the square of the shear rate. It is worth noting that all theories based on molecular concepts also predict similar behavior. The above formula (1) for the departure from Stokes law is of a similar type.

Cygan's experiments suggest that formula (1) does not hold or that the range of its validity is well below that of the data. His results suggest that the departure from Stokes law is not only linear but exponential in $F/6\pi a^2$. These findings are not entirely new, but are a much more accurate verification of the results of Turian (see Reference 6 in Cygan's paper). Turian's data are sufficiently inaccurate that one cannot distinguish whether the departure is linear or quadratic. Linear departure from constant viscosity has been reported by many authors who have measured the viscosity function in a shear flow. Unfortunately viscometric data tend to be inaccurate at the low shear rates needed to verify the law of departure. There is no corresponding loss of accuracy in Cygan's falling sphere data.

The interpretation of data to find a law of departure is always difficult, and ideally one would determine all fluid parameters from independent experiments. Unfortunately the practical limitations on carrying out viscometric experiments of comparable accuracy are formidable. However, here the falling sphere experiment has a consistency check in the form of equation (2). For a given sphere values of U are measured in several cylinders, and plotted against $W(a/R)/R$. Linearity indicates the error terms in equation (2) are negligible. From the slope μ_0 can be calculated independently of the value obtained via equation (1). Cygan has shown that even though the plots are linear the values of μ_0 become smaller as the size and density of the sphere increase. This indicates that the non-Newtonian terms play a much stronger role than the error term in equation (2) suggests.

It is this inconsistency, together with the viscosity measurements of other workers, which leads one to believe that the Rivlin-Ericksen theory is not adequate for the description of the departure from Newtonian behavior. As a result I am now investigating new theories which can correct this inconsistency. The calculations which are required for the reinterpretation of Cygan's data are complicated, and will not be completed for a long time.

II. Rotating Spheres

An experimental study of the rotational drag on a sphere was initiated by B. Mena, and his results are given in the second paper referred to above. In Mena's work a sphere was held stationary at the center of cylindrical container of fluid which rotated about its axis. The torque was measured by the angular deflection of the trifilar suspension which supported the sphere. The paper deals only with experiments on Newtonian fluids which were used to test the capabilities of the apparatus. In particular, Collins formula for the torque at low rotational Reynolds number is in good agreement with the data up to about $R = 25$. This formula is

$$\frac{\rho L}{8\pi\mu^2 a} = R \left\{ 1 + \frac{R^2}{1200} - 1.086 \left(\frac{R^2}{1200} \right)^2 + \dots \right\}, \quad (3)$$


where L is the torque, ρ and μ the fluid density and viscosity, and a is the sphere radius. An "improved" version of Collins formula is


$$\frac{\rho L}{8\pi\mu^2 a} = R \left\{ 1 + \frac{R^2/1200}{1+1.086R^2/1200} \right\}, \quad (4)$$

which was found to give a good account of the data at Reynolds numbers in excess of 100. The improved formula (4) is derived by standard methods for accelerating the convergence of an alternating series.

Mena also carried out a few measurements with a polymer solution. However, the apparatus needs some improvements before consistently reproducible data can be obtained.

Prepared by:


Bruce Caswell
Associate Professor
of Engineering


Carl Cometta
Executive Officer
Division of Engineering

BC:gb

Brown Univ

NGL-40-002-053

MEASUREMENT OF THE ROTATIONAL DRAG
ON A SPHERE AT LOW, FINITE REYNOLDS NUMBER

by

Bruce Caswell and Baltasar Mena

Division of Engineering and
Center for Fluid Dynamics
Providence, Rhode Island

1. Introduction

The torque on a sphere rotating in an unbounded fluid was first calculated by Stokes [1851] for the inertialess case. Several authors (Bickley [1938], DiFrancia [1950], Khamrui [1956], Ovseenko [1960]) have carried out expansions in powers of the Reynolds number which in the third term result in a correction to the Stokes torque. Recently, Collins [1956] has extended the calculation to the fifth term, and has obtained the torque L as

$$\frac{\rho L}{8\pi\mu^2 a} = R \left\{ 1 + \frac{R^2}{1200} - 1.086 \left(\frac{R^2}{1200} \right)^2 + O(R^6) \right\}. \quad (1.1a)$$

The regularity of this series permits its inversion which can be written as

$$\frac{\rho a^2 \Omega_\infty}{\mu} = R_s \left\{ 1 - \frac{R_s^2}{1200} + 4.086 \left(\frac{R_s^2}{1200} \right)^2 + O(R_s^6) \right\}, \quad (1.1b)$$

where μ is the viscosity, ρ the density and a the sphere radius. The rotational Reynolds numbers R and R_s are $\rho a^2 \Omega_\infty / \mu$ and $\rho L / 8\pi\mu^2 a$ respectively, and Ω_∞ is the angular velocity when the sphere spins in an unbounded fluid. Collins proved that the series within the braces contains only even powers of the Reynolds number. The alternating signs in (1.1b) suggest the use of Shanks [1955] transformation for accelerating the convergence of a slowly convergent series. Hence an "improved" version of (1.1a) is found to be

$$\frac{\rho L}{8\pi\mu^2 a} \approx R \left\{ 1 + \frac{R^2/1200}{1+1.086R^2/1200} \right\} \quad (1.2)$$

In order to compare these formulae with experimental torque-angular velocity data it is necessary to correct for the effects of container

boundaries. It will be shown later that for any configuration of rotating body and container with axial and fore-and-aft symmetry Ω_∞ is given by

$$\Omega_\infty = \Omega + K_{12} L / 8\pi\mu_0 \ell^3 + O(\Gamma^3 \ell^{-5} \text{Log} \ell) , \quad (1.3)$$

where ℓ is the container dimension, and K_{12} is a parameter which depends only on the container geometry. For the closed, finite cylinder of the experiments described below ℓ is the radius, and K_{12} has been calculated by Mena [1969] as a function of r_0/h , the radius to height ratio. In the limit of zero Reynolds number Ω_∞ is linearly related to L by Stokes law (the first term of (1.1)). It is then a simple matter to invert (1.3) and recover a formula due to Brenner [1962] which expresses the container effect as a correction to the torque. However, it should be carefully noted that at finite Reynolds number Ω_∞ is a nonlinear function of L , and hence no easy inversion of (1.3) can be obtained to give a torque correction formula.

Mena [1969] has measured Ω and L for a sphere located in the center of a finite, closed cylinder in the apparatus shown in Figure 3. From these data values of Ω_∞ were calculated with (1.3) and were then plotted in Figure 1 as $\rho L / 8\pi\mu^2$ against R . The curves were calculated from (1.1a) and (1.2). The densities and viscosities of the silicone fluids used in the experiments were determined independently; hence Figure 1 is free from any fitted parameters. The data confirm the rule that the first correction to Stokes law is valid for R up to about 15. The addition of Collins' R^5 term extends the range to at most 25. Despite the paucity of data in the high range it appears that the "improved" formula (1.2) gives a rather good account even at R about 100.

2. The Effect of Walls at Finite Reynolds Number

The analysis for the wall effect is restricted to configurations in which both the rotating body and the container are concentric, coaxial surfaces of revolution with fore-and-aft symmetry. Such symmetry guarantees that the body will experience no net force and that no net flow will result. As in the unbounded case \bar{V} , p , the velocity and pressure fields, are expanded as

$$\bar{V} = \bar{V}_1 + \bar{V}_2 + \bar{V}_3 + \dots, \quad (2.1a)$$

$$p = p_1 + p_2 + p_3 + \dots. \quad (2.1b)$$

In dimensionless form the \bar{V}_i , p_i fields would be $O(R^{i-1})$, and in dimensional form they satisfy inhomogeneous Stokes equations

$$0 = -\nabla p_i + \mu \nabla^2 \bar{V}_i + \nabla \cdot \bar{\tau}_i, \quad (2.2)$$

where the inhomogeneous "stress tensors" $\bar{\tau}_i$ are obtained by substitution of (2.1) into the Navier-Stokes equation. When the usual procedures for regular perturbations are followed the first few $\bar{\tau}_i$ are found to be

$$\bar{\tau}_1 = 0, \quad \bar{\tau}_2 = -\rho \bar{V}_1 \bar{V}_1, \quad \bar{\tau}_3 = -2\rho [\bar{V}_1 \bar{V}_2]_s, \quad \text{etc.} \quad (2.3)$$

The brackets $[]_s$ denote the symmetric part of a dyadic.

It is evident from the structure of the $\bar{\tau}_i$ that the Navier-Stokes equation has been written relative to an origin fixed at the geometric center. Hence the boundary conditions on the velocity perturbations are

$$\bar{V}_i = \bar{\Omega}_i \times \bar{r} \quad \text{on } B, \quad \bar{V}_i = 0 \quad \text{on } C, \quad (2.4)$$

where B denotes the surface of the rotating body and C that of the container. The $\bar{\Omega}_i$ are directed along the symmetry axis, and are determined by the integrals

$$\int_B \bar{\mathbf{r}} \times \bar{\mathbf{t}}_i dA = - \int_C \bar{\mathbf{r}} \times \bar{\mathbf{t}}_i dA = \delta_i(\bar{L}) , \quad (2.5)$$

where

$$\delta_1(\bar{L}) = \bar{L} , \quad \text{and for } i > 1 \quad \delta_i(\bar{L}) = 0 . \quad (2.6)$$

The stress vector perturbations $\bar{\mathbf{t}}_i$ are calculated from

$$\bar{\mathbf{t}}_i = -\bar{n} p_i + \mu \frac{\partial \bar{V}_i}{\partial n} , \quad (2.7)$$

in which the unit normal vector \bar{n} is directed out of the fluid surface. The equality of the integrals over both B and C in (2.5) follows from (2.2), the divergence theorem and the axial symmetry which ensures that $\bar{n} \cdot \bar{\Omega} \times \bar{\mathbf{r}}$ is zero on B . The fore-and-aft symmetry ensures that the surface integrals of the $\bar{\mathbf{t}}_i$ vanish for all i on both B and C . The general pattern of the motions represented by the \bar{V}_i can also be deduced from the symmetry. It can be shown in a manner similar to that used by Collins [1956] that for i odd the fluid particles move in circles about the spin axis and for i even the streamlines are distributed in the meridional planes in such a way that no net flow occurs.

The perturbation scheme outlined above is unusual in one important respect. Instead of the torque function $L(\Omega)$, for example (1.1a), it yields the inverse torque function $\Omega(L)$. Thus it is usual to satisfy the boundary conditions (2.4) with $\bar{\Omega}_1$ set equal to $\bar{\Omega}$ and all higher order $\bar{\Omega}_i$ then vanish. The torque integrals (2.5) are then used to

calculate $L(\Omega)$. In the inverse scheme the torque integral for $i = 1$ is set equal to the total torque L , and by (2.6) the higher order integrals are forced to be zero. As will be seen below the inverse method has special advantages for the calculation of wall effects because of the far field properties of the $\bar{V}_{\infty i}$, $P_{\infty i}$ fields.¹ It should be noted that if dimensionless variables are employed the appropriate Reynolds number in (2.1) will be one based on the Stokes spin $\Omega_{\infty 1}$ rather than the total spin Ω_{∞} . For the sphere it can be seen from (1.1b) that this inverse Reynolds number is $\rho L / 8\pi\mu^2 a$.

Since (1.3) can be written as a formula which gives Ω as a correction to Ω_{∞} it is useful at this point to examine the nature of the $\bar{V}_{\infty i}$ fields. From the fundamental solution of the linear Stokes equation and the symmetry of B it can be shown that

$$\bar{V}_{\infty 1} = -\bar{L} \times \bar{r} / 8\pi\mu r^3 + O(r^{-3}). \quad (2.8)$$

If B lacks fore-and-aft symmetry or does not spin about its own axis other terms of $O(r^{-2})$ must be added (Brenner [1964a]). For the sphere the leading term in (2.8), called a "rotational Stokeslet," is $\bar{V}_{\infty 1}$ exactly. For $i > 1$ the first few $\bar{V}_{\infty i}$ are known only for the sphere. However, it is possible to deduce from the structure of $\bar{T}_{\infty 2}$ (2.3) that the leading term in (2.8) will give a particular integral to (2.2) of $O(r^{-3})$; hence any terms of $O(r^{-2})$ in $\bar{V}_{\infty 2}$ must satisfy the homogeneous Stokes equation. Since $\bar{V}_{\infty 2}$ must be bilinear in $\bar{\Omega}_{\infty 1}$ and lie in the

¹All quantities with the subscript ∞ are associated with the case of an unbounded fluid.

meridional planes it must have the form

$$\bar{v}_{\infty 2} \sim \left\{ \bar{\Omega}_{\infty 1}^2 - 3(\bar{\Omega}_{\infty 1} \cdot \bar{r})^2 / r^2 \right\} \rho a^5 \bar{r} / 8\mu r^3 + o(r^{-3}) . \quad (2.9)$$

From Collins' [1956] work it can be shown that for the sphere the proportionality can be replaced by an equality. For i even, the asymptotic form of the remaining $\bar{v}_{\infty i}$ will be similar to (2.9) with the leading term multiplied by $\bar{\Omega}_{\infty 1}^{i-2}$. For i odd, it can be shown from (2.2), (2.8), and (2.9) that

$$\bar{v}_{\infty i} \sim \bar{\Omega}_{\infty 1} \times \bar{r} g(\bar{\Omega}_{\infty 1}^{i-1} r^{-4}) + o(r^{-4}) , \quad (2.10)$$

where g is a scalar function of $\bar{\Omega}_{\infty 1}$ and \bar{r} which is $o(\bar{\Omega}_{\infty 1}^{i-1} r^{-4})$.

The advantage of the inverse perturbation scheme now becomes apparent.

It will be seen below that the lowest order term which interacts with the container is the rotational Stokeslet of (2.8). That none of the $\bar{v}_{\infty i}$ for $i > 1$ can contain such a term follows from the integral conditions (2.5) when C recedes to infinity. Hence the bookkeeping is greatly simplified in the double expansion to be used for the wall effect calculation.

Each of the fields \bar{v}_i , p_i in (2.1) is expanded as

$$\bar{v}_i = \bar{v}_{i1} + \bar{v}_{i2} + \bar{v}_{i3} + \dots , \quad (2.11a)$$

$$p_i = p_{i1} + p_{i2} + p_{i3} + \dots . \quad (2.11b)$$

The boundary conditions (2.4) are satisfied by a slight modification of the method of reflections (Brenner [1962]) as

$$\bar{v}_{i1} = \bar{\Omega}_{\infty 1} \times \bar{r} \quad \text{on } B , \quad \bar{v}_{i1} \rightarrow 0 \quad \text{as } r \rightarrow \infty \quad (2.12a)$$

$$\bar{V}_{i2} = -\bar{V}_{i1} \quad \text{on } C, \quad (2.12b)$$

$$\bar{V}_{i2} + \bar{V}_{i3} = \delta\bar{\Omega}_{i2} \times \bar{r} \quad \text{on } B, \quad \bar{V}_{i3} \rightarrow 0 \quad \text{as } r \rightarrow \infty, \quad (2.12c)$$

$$\bar{V}_{i4} = -\bar{V}_{i3} \quad \text{on } C, \quad (2.12d)$$

$$\bar{V}_{i4} + \bar{V}_{i5} = \delta\bar{\Omega}_{i4} \times \bar{r} \quad \text{on } B, \quad \bar{V}_{i5} \rightarrow 0 \quad \text{as } r \rightarrow \infty, \quad (2.12e)$$

etc. Expansions similar to (2.11) are also written for the $\bar{\tau}_i$ as

$$\bar{\tau}_i = \bar{\tau}_{i1} + \bar{\tau}_{i2} + \bar{\tau}_{i3} + \dots \quad (2.13)$$

The $\bar{\tau}_{ij}$ are identified by substitution of (2.11a) into (2.3). Superficially the process of identification appears to be somewhat arbitrary. However, an inspection of the boundary conditions (2.12) reveals certain properties of the \bar{V}_{ij} which suggest a rational choice for the $\bar{\tau}_{ij}$. For j even it is clear from (2.12b,d) that the \bar{V}_{ij} fields are defined everywhere within C including the interior of B . Thus the identification of the $\bar{\tau}_{ij}$ is made by selecting products which are defined within B for j even and outside B for j odd. For example, for $i = 2$ the first few $\bar{\tau}_{2j}$ are:

$$\begin{aligned} \bar{\tau}_{21} &= -\rho \bar{V}_{11} \bar{V}_{11}, \quad \bar{\tau}_{22} = -\rho \bar{V}_{12} \bar{V}_{12}, \\ \bar{\tau}_{23} &= -2\rho [(\bar{V}_{11} + \bar{V}_{13})(\bar{V}_{12} + \bar{V}_{13})]_s, \quad \bar{\tau}_{24} = -2\rho [\bar{V}_{14}(\bar{V}_{12} + \bar{V}_{14})]_s, \\ \bar{\tau}_{25} &= -2\rho [(\bar{V}_{11} + \bar{V}_{13} + \bar{V}_{15})(\bar{V}_{14} + \bar{V}_{15})]_s, \quad \text{etc.} \end{aligned} \quad (2.14)$$

The torque integral (2.5) for \bar{V}_{11} , p_{11} is set equal to \bar{L} , and equal to zero for the remaining fields. It is obvious from (2.12a) and (2.14) that the \bar{V}_{i1} , p_{i1} are identical to the $\bar{V}_{\infty i}$, $p_{\infty i}$. A glance

at (2.14) shows clearly the rapid increase in complexity of the $\bar{\tau}_{ij}$ as j increases. However, by ordering the terms in powers of ℓ^{-1} , the reciprocal container dimension, it is possible to keep the complexity within bounds. As will soon become apparent only a few of the \bar{v}_{ij} need to be considered to obtain a correction to $O(\ell^{-3})$ such as that in (1.3).

As in Brenner's [1962, 1964] work regularity in \bar{r} for the \bar{v}_{ij} with j even is invoked to expand these fields in a Taylor's series about an origin in B . These Taylor expansions can be separated into the sum of a rigid motion and a regular non-rigid motion. In order to satisfy the rigid motion requirement on B it is necessary to add fields which on B cancel the non-rigid parts. This is accomplished with the fields of j odd as can be seen by inspection of (2.12c,e). For the homogeneous Stokes equation it was shown by Brenner [1962] that the far field behavior of $\bar{v}_{\infty 1}$ requires \bar{v}_{12} to be of the form

$$\bar{v}_{12} = \delta\bar{\Omega}_{12} \times \bar{r} + O(\ell^{-5}), \quad (2.15)$$

where

$$\delta\bar{\Omega}_{12} = -K_{12} \bar{L} / 8\pi\mu\ell^3. \quad (2.16)$$

The constant K_{12} is a pure number dependent only on the shape of C . Since \bar{v}_{12} is essentially a rigid motion it follows from (2.12c) that the \bar{v}_{ij} , $j > 2$, are at most $O(\ell^{-5})$, and hence need not be considered any further.

It is easily shown that the particular integral of the governing equation (2.2) with $\bar{\tau}_{22}$ (2.14) evaluated with (2.15) is a hydrostatic pressure. Hence to $O(\ell^{-5})$ \bar{v}_{22} consists only of a complementary function. From (2.12b) and (2.9) it follows that \bar{v}_{22} is a regular field

of the form

$$\bar{V}_{22} = \rho a^5 K_{22} \bar{\mathbf{r}} \cdot \bar{\mathbf{S}} / \mu \ell^3 + o(\ell^{-3}), \quad (2.17)$$

where the symmetric shear field gradient is given by

$$\bar{\mathbf{S}} = \bar{\Omega}_{\infty 1}^2 - 3\bar{\Omega}_{\infty 1} \bar{\Omega}_{\infty 1}, \quad (2.18)$$

and K_{22} is a number which depends on the geometry of both B and C .

The condition (2.12c) of rigid motion on B requires \bar{V}_{23} to satisfy the boundary conditions

$$\bar{V}_{23} = -\rho a^5 K_{22} \bar{\mathbf{r}} \cdot \bar{\mathbf{S}} / \mu \ell^3 \text{ on } B, \quad \bar{V}_{23} \rightarrow 0 \text{ as } r \rightarrow \infty. \quad (2.19)$$

The only term of $o(\ell^{-3})$ in \bar{V}_{23} (2.14) comes from the product $\bar{V}_{11} \bar{V}_{12}$ which gives a particular integral whose leading term is $o(r^{-2} \ell^{-3})$.

This ensures that \bar{V}_{24} and all subsequent terms are at most $o(\ell^{-5})$.

When the argument is carried forward to the \bar{V}_{3j} fields it can be shown that no terms of $o(\ell^{-3})$ are contributed. In the first place \bar{V}_{32} contains no such term because of (2.10) and (2.12a). Secondly when the \bar{V}_{3j} are worked out similarly to (2.14) it can be shown that \bar{V}_{12} and \bar{V}_{22} can make no contribution of $o(\ell^{-3})$ to the \bar{V}_{3j} . Similar remarks apply to all the remaining \bar{V}_{ij} . Hence when the $\bar{\Omega}_{ij}$ are added up their sum differs from $\bar{\Omega}_{\infty}$ by the correction given in (1.3). It remains only to remark on the nature of the error terms in (1.3). For the sphere it can be seen from Collins' [1956] work that $\bar{V}_{\infty 3}$ will introduce a term of $o(R^3 \ell^{-5} \text{Log} \ell)$. For other axisymmetric bodies the \bar{V}_j fields have not been worked out, and hence the error in (1.3) should be regarded as $o(R^3 \ell^{-4})$. While no proof is offered here it should be noted that (1.3)

holds also for non-Newtonian fluids. The proof is rather complicated, and is similar to the one given by Caswell [1970] for the correction to the translational velocity of a particle in a non-Newtonian fluid in the limit of zero Reynolds number. This analysis which is far more general than that given above also implies the existence of higher order terms containing $\log \ell$. Hence if additional terms in (1.3) are to be calculated it is clear that the regular expansions employed above must be replaced by appropriate matched asymptotic expansions.

3. Container Constants

Values of the wall-effect or container constant K_{12} needed in (1.3) are known for several geometries, and are summarized conveniently by Happel and Brenner [1965]. However, for a cylinder closed at both ends K_{12} is not available directly. Brenner [1964b] has calculated K_{12} for a cylinder closed at one end and with a free plane surface (zero shear stress) at the other. It follows from the linearity of the Stokes equation that Brenner's solution also satisfies the problem of two point torques located symmetrically in a closed container as shown in Figure 2. In the limit of large b_1 and r_0 the situation reduces to that of a composite body made of the two point torques separated by a distance $2b_2$ located at the center of a closed cylinder of height $2h$ and diameter $2r_0$. Note that although $b_2 \ll b_1$ it is also possible to have $b_2 \gg a$, where a is the dimension of the particle approximated as a point torque. The ratio of the torque on the composite body in the cylinder to its value in an unbounded region depends to $O(r_0^{-3})$ only on K_{12} . By taking the appropriate limits of Brenner's solution Mena [1969] has obtained this ratio, and found K_{12} as

$$K_{12}(r_0/h) = \frac{1}{16} \left(\frac{r_0}{h} \right)^3 \{ 3.6062 + S(r_0/h) \}, \quad (3.1)$$

where

$$S(x) = 64 \sum_{n=0}^{\infty} \xi_n^2 K_1(2\xi_n x) / I_1(2\xi_n x), \quad (3.2)$$

$$\xi_n = (2n+1)\pi/4, \quad (3.3)$$

and $K_1(\)$ and $I_1(\)$ are modified Bessel functions of the first kind.

It should be noted that (3.1) is written with ℓ in (1.3) taken to be r_0 .

The following table shows that the ends have a pronounced effect only for $r_0/h > 1$.

TABLE I

Container Constants for a Closed Cylinder

r_o/h	K_{12}
0	0.79682
1/2	0.79960
1	0.81938
2	1.9516
4	14.427
∞	$\frac{3.6062}{16} (r_o/h)^3$

4. Torque Measurements with a Trifilar Suspension

Torque measurements were carried out with the apparatus of Figure 3 in which the sphere was held stationary and the cylinder was rotated. The latter was made of precision glass tubing, and the aluminum end plates were held with tie rods. A portion of the top was removable in order to introduce the spheres and the fluid. The support shaft for the sphere was attached at the center of a small horizontal platform which was suspended from three symmetrically placed cords. These were secured to a horizontal support disk located at a large distance above the cylinder top, and whose center coincided with the axis of rotation. The torque induced by rotation produced an angular displacement of the sphere which was measured optically. Since the direction of rotation was reversible the angular displacement of the sphere was amplified by a factor of four.

With the support wires assumed to behave as inextensible, perfectly flexible cords the torque L on the sphere is related to the angular displacement θ by a static torque balance which gives

$$L = Wr_1r_2 \sin \theta / \sqrt{z^2 - 2r_1r_2(1 - \cos \theta)}, \quad (4.1)$$

where r_1 and r_2 are the radial positions of the chords on the platform and support disk respectively, z is the vertical distance between them, and W is the net vertical force. It can be shown that errors which result from the neglect of the elongation and twist of the wires were less than 0.1 per cent in the worst case.

As long as the configuration of the body and container together has a plane of equatorial symmetry it follows from the above analysis for wall wall effects that W is the weight of the sphere assembly supported by the

wires less the bouyancy of the immersed parts. Hence the shaft introduces an error in W by disturbing the symmetry, and an error in the hydrodynamic torque as given by (1.1). Cox [1965] has shown that the hydrodynamic force which arises from lack of fore-and-aft symmetry is $O(R^2)$ as $R \rightarrow 0$. Further analysis suggests that the force is also proportional to the ratio of the shaft cross section to the projected area of the sphere. The torque produced by the shaft was estimated by multiplication of the wetted length by the torque per unit length for an infinite cylinder. The effects of these errors were investigated by carrying out measurements with shafts of $1/16$ and $1/32$ inch diameter for each of the spheres whose diameters varied from 1 to $3/2$ inches. No appreciable error was observed over most of the Reynoldsnumber range.* However, at the higher values a definite trend appeared in which the thicker shafts gave higher torque readings for a given rotational speed.

Three different silicone fluids were used and their viscosities (0.498, 1.85, and 0.252 poise) were determined in a Rotovisco viscometer. The excellent agreement between the data and the analytical curve in the Stokes regime suggests the use of the configuration of Figure 3 as a viscometer. The viscosity temperature coefficients of these fluids are small enough so that a constant temperature bath was not needed. The experiments were carried out in a room whose temperature was maintained at $25 \pm 1^\circ\text{C}$.

The discrepancy between the experimental points in Figure 3 and the calculated curve is less than one per cent in the Stokes regime, two per cent in the regime of Collins' formula (1.1) and about five per cent for the highest Reynolds numbers. The departure at the highest values may be a reflection

*Mena [1969] carried out flow visualization studies of the secondary flows which showed no visible disturbance of equatorial symmetry due to the shaft.

of the approximate nature of (1.2). However, as the Reynolds number was increased a torsional oscillation of the sphere was observed, and this ultimately limited the range of observation. This instability was probably caused by slight misalignment between the sphere and the cylinder axes. Beyond Reynolds number 30 the data are not sufficiently accurate to provide a verification of the wall-effect formula (1.3). Clearly at some point the term of $O(R^3 \ell^{-5} \log \ell)$ in (1.3) should become appreciable. Below $R = 30$ the uncorrected points (not shown) all lie to the left of the calculated curves which indicates the validity of (1.3) up to that point. For the higher Reynolds numbers the curve calculated from (1.2) lies midway between the corrected and uncorrected points. However, it is not possible to say whether the discrepancy is due to the failure of the approximate torque formula (1.2) or the wall correction (1.3).

The support of this work by the National Science and Space Administration under ~~grant NSR #0~~ is gratefully acknowledged. Partial support of B. M. by the Instituto Nacional de la Investigacion Cientifica (Mexico) is also acknowledged.

REFERENCES

- Bickley, W. G. [1938], Phil. Mag. [7] 25, 746.
- Brenner, Howard [1962], J. Fluid Mech., 12, 35.
- Brenner, Howard [1964a], J. Fluid Mech., 18, 144.
- Brenner, Howard [1964b], Appl. Sci. Res. (Ser. A), 13, 81.
- Caswell, Bruce [1970], Chem. Eng. Sci. (in press).
- Collins, W. D. [1956], Mathematika, 2, 42.
- Cox, R. G. [1965], J. Fluid Mech., 23, 273.
- DiFrancia, G. T. [1950], Boll. Unione Mat. Ital., [3] 5, 273.
- Happel, John and Brenner, Howard [1965], "Low Reynolds Number Hydrodynamics," Prentice-Hall, Englewood Cliffs, New Jersey, p. 350.
- Khamrui, S. R. [1956], Bull. Calcutta Math. Soc., 48, 159.
- Mena, Baltasar [1969], M.Sc. Dissertation, Division of Engineering, Brown University, Providence, R. I.
- Ovseenko, Yu, G. [1960], Tr. Novocherk. Politekhn. Inst., 109, 51.
- Shanks, D. [1955], J. Math. and Phys., 34, 1.
- Stokes, Sir G. G. [1851], "On the Effect of Internal Friction on the Motion of Pendulums," Camb. Trans. IX [8].

BC:gb
3/6/70

CAPTIONS FOR FIGURES

Figure 1. Non-dimensional torque vs. Reynolds number. a) Low Reynolds regime; b) High Reynolds regime. - - - - Stokes, - - - - Stokes plus first correction, ——— Collins, ---- Eqn. (1-2). Open points are corrected for wall effects. Solid points are uncorrected.

Figure 2. Definition sketch for the calculation of wall effects in a closed cylindrical container.

Figure 3. Schematic view of experimental apparatus using a tri-filar suspension system for torque measurement.

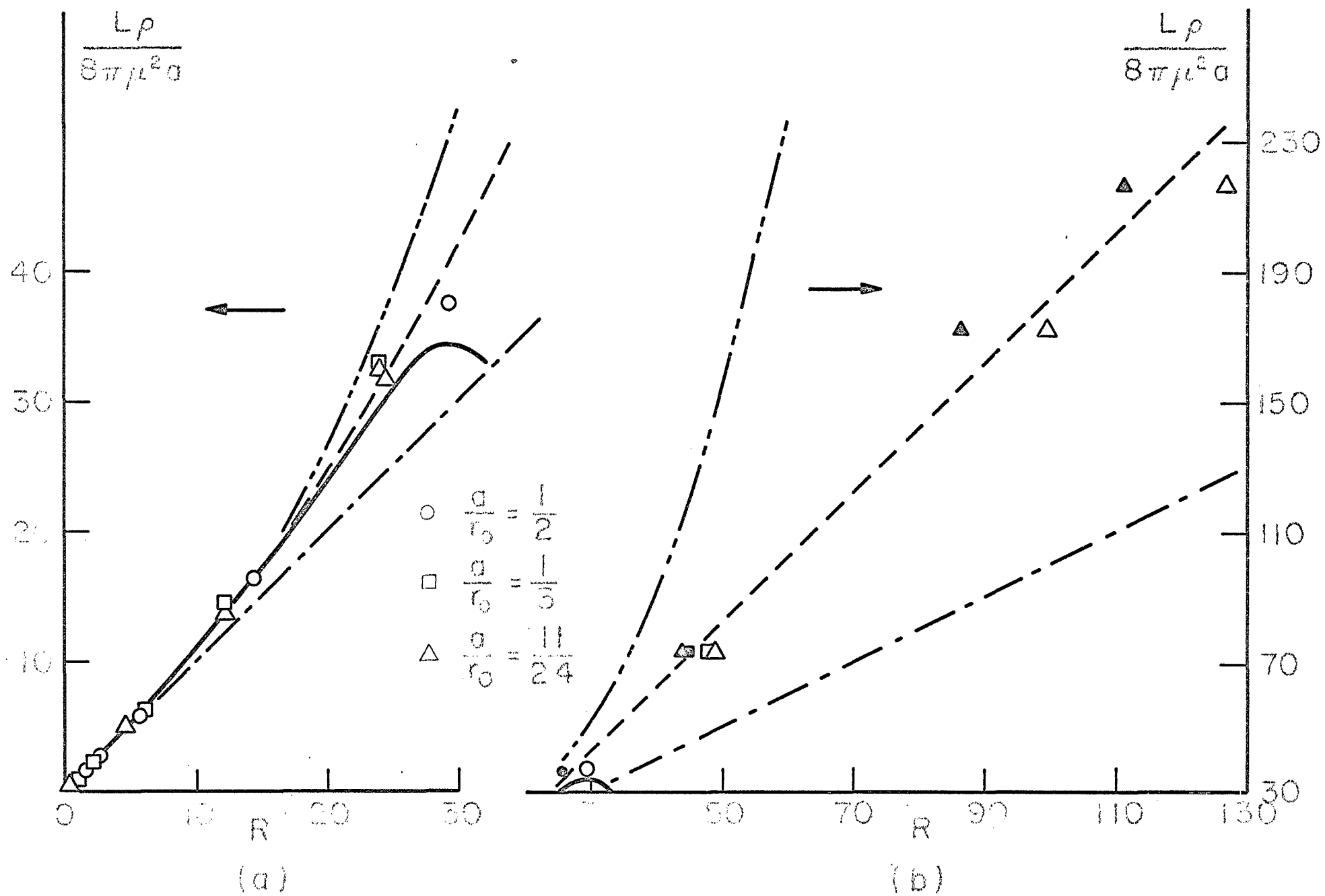


FIGURE 1

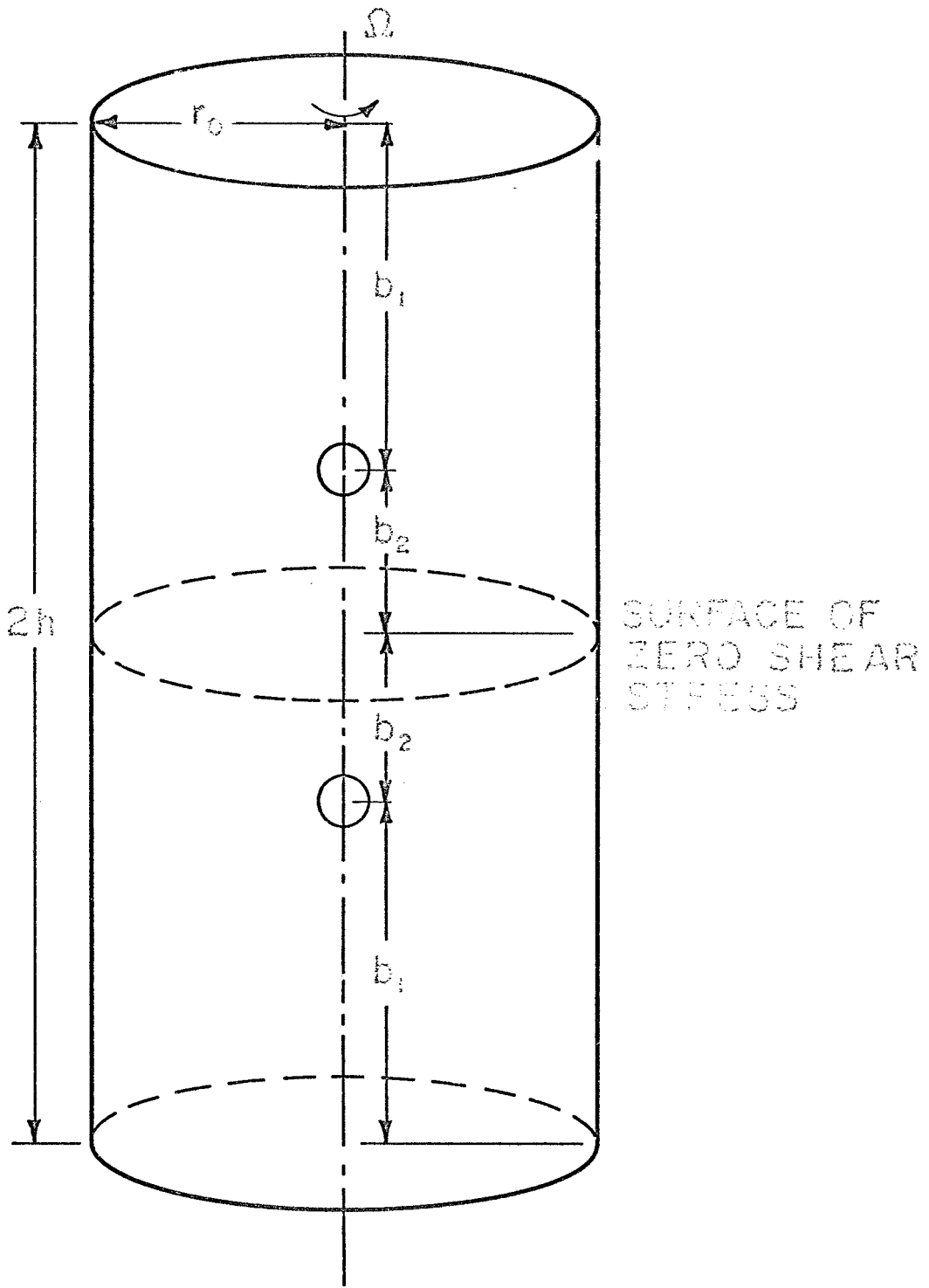


FIGURE 2

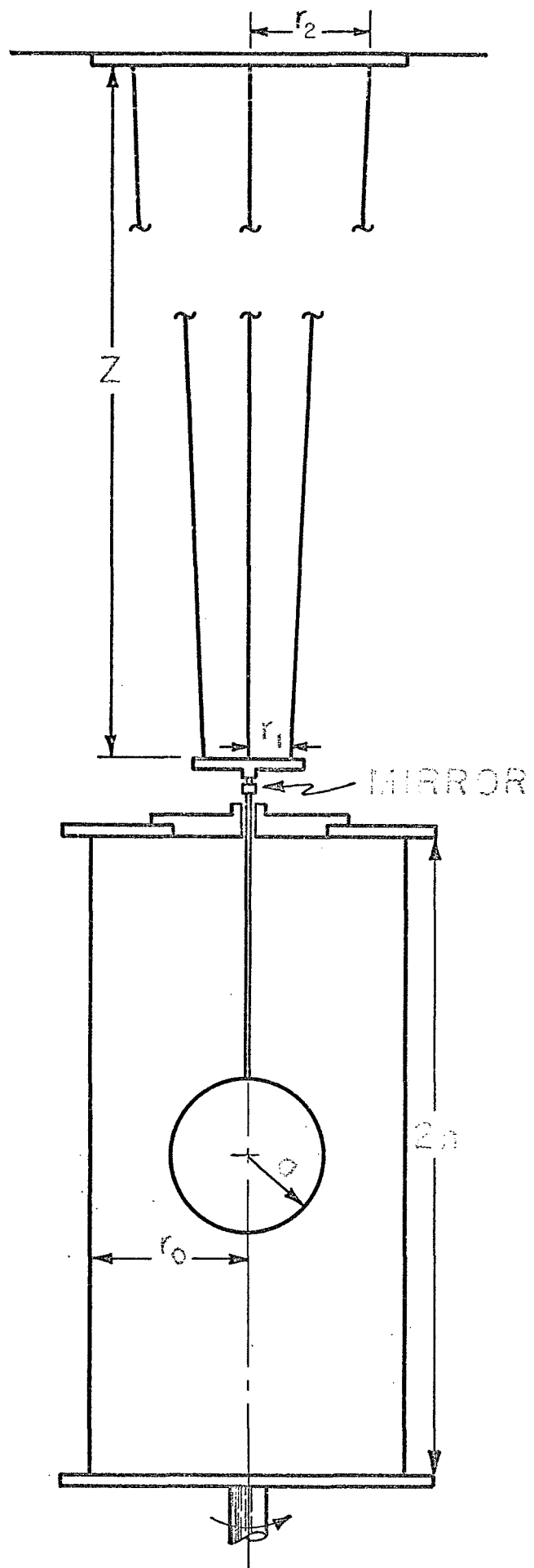


FIGURE 3

Precision Falling Sphere Viscometry

David A. Cygan

and

Bruce Caswell

Brown University, Providence, Rhode Island

NGL-40-002-053

SYNOPSIS

Terminal velocity data of spheres falling in a polyisobutylene (PIB) solution were obtained in sealed tubes. The tubes were easily invertible so that the fall of a sphere could be repeated as often as desired. The sealed tubes have the further advantage that degradation of the fluid is greatly reduced when compared to similar experiments in open tubes. Precisely reproducible velocities were obtained by careful temperature control and by measurement of the radial eccentricity. From such data it is possible to calculate the zero-shear viscosity, μ_0 , provided the range of effective shear rates is sufficiently small. To acquire data in this range it is necessary to use spheres with small effective mass (actual mass less the mass of the displaced fluid). Spheres of various materials (nylon, ruby, steel, and carbide) were used, and their properties were checked by dropping them in a Newtonian fluid of known viscosity. In some cases the sphere properties were found to fall outside the tolerances specified by the manufacturers. A test of the

absolute accuracy of the falling sphere method was made with a calibrated oil supplied by the Cannon Instrument Company. The viscosity measured with the spheres is within half a percent of the value specified.

The data have been analyzed with formulae derived from perturbation calculations based on the theory of Rivlin-Ericksen fluids. These formulae include the effects of walls and fluid inertia. The third order theory predicts the initial departure from Stokes law. Ideally μ_0 can be obtained by extrapolation of data in the range of the third order theory. However, for the PIB solution this range appears not to exist or else it falls below that of most of the data. Since the above extrapolation was not feasible, data were taken in tubes of four sizes, and μ_0 was then deduced from the wall effect formulas. The value so obtained was found to be in good agreement with the values obtained from an extrapolation which assumes the apparent viscosity based on Stokes law varies exponentially with the shear stress. This type of limiting behavior contradicts the third order theory but describes the data remarkably well.

1. INTRODUCTION

The perturbation calculations of Leslie,¹ Giesekus,² and Caswell and Schwarz³ for the motion of a sphere falling in a third order Rivlin-Ericksen fluid predict for a non-Newtonian fluid the initial departure from Stokes law. The recent analyses of Caswell^{4,5} take into account the effect of finite container boundaries on the motion of the sphere. From the falling sphere data of Turian,⁶ Caswell⁴ was able to calculate the zero shear viscosity of a polymer solution either by extrapolating the sphere data to zero shear rate or by computing the effect of the tube walls on the terminal velocity. These values agreed mutually to within about 1 per cent, but differed by about 4 per cent from the value Turian obtained from an empirical extrapolation. These results suggested that the falling sphere experiment could be useful in the measurement of the zero-shear viscosity. While the interpretation of these data according to the third order theory possesses some self-consistency, it cannot be argued unequivocally that Turian's empirical extrapolation is without validity. This extrapolation implies a different departure from Stokes law than that predicted by the third order theory.

In order to further investigate these effects it was decided to attempt to make highly precise and reproducible terminal velocity measurements of spheres falling through a solution of polyisobutylene in cetane. Spheres of nylon, ruby, steel and carbide were used to provide a wide range of shear stress and to check the boundary conditions at the sphere's surface from one material to another. The data were taken in four tubes of different size in order to determine the effect of the walls upon the motion. Each tube was sealed to protect the fluid from depolymerization

and to facilitate the repetition of data. With a sphere inside the closed tube, the fall speed could be repeated many times by inverting the tube as one would turn over an hourglass. Provisions were made to measure the radial eccentricity of the falling sphere in order to correct the velocity to the center line value. An average speed with a small standard deviation was calculated from the data for each sphere, and the results were interpreted according to the available theory.

2. THEORY

For the purpose of the falling sphere experiment it is convenient to express the resistance of a particle moving through a fluid in terms of a terminal velocity function $U_{\infty}(F)$, where F is the net hydrodynamic force on the particle. In the inertialess flow regime the third order theory analyses referred to above yield $U_{\infty}(F)$ for the sphere in the form

$$U_{\infty}(F) = U_s \left[1 - \left(\frac{\lambda}{\mu_0} \right)^2 \left(\frac{F}{6\pi a^2} \right)^2 + o \left(\frac{F}{6\pi a^2} \right)^4 \right], \quad (1)$$

where

$$U_s = F/6\pi a \mu_0 \quad (2)$$

is the Stokes velocity, a is the sphere radius, and μ_0 is the zero-shear viscosity. Here λ is a characteristic time which depends on the fluid properties and the geometry of the particle. It was shown by Caswell⁴ that virtually all the theories of the stress tensor for isotropic fluids which are currently in vogue will yield the same law of departure from Stokes law as given by eq. (1). Caswell also showed that once λ is known in terms of the parameters of the third order fluid it can be expressed in terms of the parameters of any other theory without

detailed perturbation calculations.

Experimental terminal velocities are expressible in terms of an apparent viscosity μ based on Stokes law; from eq. (1) $1/\mu$ is given by

$$\frac{1}{\mu} = \frac{6\pi a U_{\infty}}{F} = \frac{1}{\mu_0} - \frac{(\lambda\tau)^2}{\mu_0^3} + O(\tau^4), \quad (3)$$

where $\tau = F/6\pi a^2$ is a characteristic shear stress (for the Newtonian case $3\tau/2$ is the equatorial or maximum shear stress). Hence a plot of $1/\mu$ against τ^2 should become linear with intercept $1/\mu_0$ in the limit of zero shear stress.

The effect of container boundaries upon the motion of a particle moving in a viscoelastic fluid is given by Caswell⁴ as a correction to \bar{U}_{∞} , the terminal velocity in an unbounded fluid, by

$$\bar{U} = \bar{U}_{\infty}(\bar{F}) + \bar{k} \cdot \bar{F}/6\pi\mu_0\ell + O(\ell^{-2}). \quad (4)$$

For the purposes of this paper a particle is a body whose size is small enough to satisfy the inertialess flow requirement of Reynolds number $\ll 1$. The experiments presented here cover a Reynolds number range of 10^{-2} to 10^{-6} which is well within the inertialess domain. The particle is located at a distance ℓ from the wall, and \bar{k} is the wall-effect tensor of Brenner.⁷ This first order wall correction can be shown to be independent of both the shape of the particle and the velocity boundary condition on its surface. For instance, it holds for a solid sphere both with and without slip and also for a fluid sphere with internal circulation.

The result expressed by eq. (4) was derived from a general perturbation analysis. Higher order terms in $1/\ell$ can be obtained only with calculations of considerable complexity. When these terms are already known in the

Newtonian theory they can be easily included. Thus when a sphere translates along the axis of a circular tube of radius R under the influence of an axial force F its velocity U is given by

$$U = U_{\infty}(F) - \frac{F}{6\pi\mu_0 R} W(a/R) + O\left(\frac{F}{R}\right)^3, \quad (5)$$

where the function $W(a/R)$ is obtained from Faxen's series as worked out by Bohlin⁸ and is given by

$$W(a/R) = 2.1044 - 2.0888(a/R)^2 + 0.9481(a/R)^4 \\ + 1.372(a/R)^5 - 3.87(a/R)^7 + 4.19(a/R)^9 + \dots \quad (6)$$

When $U_{\infty}(F)$ is replaced by the Stokes velocity, eq. (2), Faxen's wall correction eq. (10) for a Newtonian fluid is recovered. Because of the linearity of Stokes law the Newtonian formula is easily inverted and expressed as a correction to the force, and it is in the form of a force correction that Faxen's formula is usually presented. For non-Newtonian fluids, only the velocity correction form eq. (5) is valid. This is evident from the work of Tanner⁹ who showed that the Faxen force formula did not adequately correct terminal velocity data taken in polymer solutions. Turian⁶ assumed the form of eq. (5) without identifying the viscosity in the denominator as μ_0 . His fall tubes and spheres were selected so that $W(a/R)$ was determined essentially by the first term in eq. (6). Turian's assumed wall correction together with his logarithmic plot of $1/\mu$ against τ (Figure 5) form the basis upon which Bird and his coworkers (see for instance Ashare¹⁰) have used the falling sphere experiment to obtain the zero-shear viscosity. It should be emphasized that the wall-effect formula, eq. (5), is derivable from theories of the stress tensor

which in the limit of slow flow are equivalent to the theory of Rivlin-Ericksen fluids (Caswell⁴). On the other hand the logarithmic plot implies a linear departure from $1/\mu_0$ in contrast to the quadratic departure expressed by eq. (3).

It is clear from the error term that eq. (5) is not uniformly valid in powers of R^{-1} . It can be shown from dimensional and symmetry arguments that the next term of $O(R^{-3})$ will modify the second term in eq. (6) so that it will be replaced by

$$- \left[2.0888 + C\kappa^2 \left(\frac{2\Delta\rho ga}{9\mu_0} \right)^2 \right] \frac{a^2}{R^2}, \quad (7)$$

where C is a numerical constant, κ is a characteristic time, $\Delta\rho$ is the sphere-fluid density difference and g is the gravitational acceleration. Hence in the falling sphere experiment where F is the difference between the gravity and buoyancy forces the error in eq. (5) can be suppressed by suitable choice of spheres. Under these circumstances μ_0 can be determined from the slope of eq. (5) by measurement of the terminal velocity of a given sphere in tubes of several sizes. For a particular fluid $U_\infty(F)$ has a characteristic value for each sphere (at constant F); thus a plot of U against $W(a/R)/R$ for several tubes will have slope $-F/6\pi\mu_0$ and intercept $U_\infty(F)$. The values of the latter for several spheres can then be used to determine μ_0 from the intercept of Eq. (3).

In high precision work it is important to accurately control the center line motion; or if it cannot be controlled, the eccentricity b from the center line should be measured. The axial speed for a particle moving under the influence of an axial force can be obtained from eq. (4) and the work of Happel and Brenner⁸ as

$$U(b/R) = U + (2.1044 - f(b/R)) \frac{F}{6\pi\mu_o R} + O(a^3 b^2 R^{-5}), \quad (8)$$

where U is the center line velocity given by eq. (5) for the sphere, and f is a function tabulated in Happel and Brenner. For small values of its argument $f(b/R)$ is given by

$$f(b/R) = 2.1044 - 0.6977(b/R)^2 + O(b/R)^4. \quad (9)$$

The eccentric position causes a sphere to rotate, and it was shown by Brenner and Happel¹¹ for Newtonian fluids that the axial velocity is unaffected by this rotation. For non-Newtonian fluids it has been shown by Caswell⁵ that in addition to the rotation the normal stresses can produce a radial migration. Working with a polymer solution Tanner⁹ had observed such a radial motion away from the center line. If the radial migration is not too large the mean value of b can be used in eq. (8). When eq. (9) is a good approximation to $f(b/R)$ the error in taking the mean value is small (see Caswell⁵).

3. EXPERIMENTAL APPARATUS

3.1 Tube Design

Four tube diameters were selected in order to investigate the wall effect upon the terminal velocity of the spheres. The diameters (2.223, 3.050, 4.445, and 7.617 cm \pm 0.0005 cm tubes #1, #2, #3, and #4 respectively) were chosen so that the influence of the walls would change by uniform increments from one size to the next. Each fall tube was closed with end plates which had 0.635 cm loading holes through their centers (see Figure 1). These holes were used to fill the tube and to change spheres. End caps,

attached by screws to the end plate, covered the loading holes and sealed the fluid from contact with the atmosphere. Excellent stability of the fluid was thus achieved by isolating it from oxygen in the air. Throughout the investigation the tubes were sealed, and the fresh fluid was kept in a closed bottle away from the light. As a check, the 4.445 cm tube was filled with the polymer solution, and sphere speeds were recorded. After an interval of nine months, the tube was refilled with a fresh sample, and the velocities of the same spheres were remeasured. The results showed a slight speed increase on the order of 0.1%. Therefore, it was concluded that depolymerization was reduced to negligible levels.

A fixed frame was used to hold each tube in a vertical position. The frame had a lower shaft with a conical tip and an upper support arm with a V-notch cut into it. The supports were aligned properly so that the end caps would fit into the supports. Each cap had a conical hole to rest on the lower shaft, and the outside diameter of the upper cap was held into the V-notch for positive alignment. With a sphere sealed in the viscometer, data was easily taken by removing the tube from the frame, inverting it, replacing it in the supports, and measuring the time as the sphere fell to the bottom. It should be kept in mind that the viscometer was designed for viscosities of 10 poises or more so that the particle motion would be slow enough to allow the tube to be inverted by hand.

Temperature control for the viscometer was provided by circulation of water through a plexiglass jacket surrounding the fall tube. The water was supplied from a constant temperature bath which maintained set values to within a tolerance of $\pm 0.01^{\circ}\text{C}$.

3.2 Velocity Measurements

The fall velocity was measured by timing the particle between two fixed points. A vertical cathetometer was used to sight on the sphere and measure the fall distance. The fall time was measured with an electronic counter equipped with a start-stop trigger. In order to insure that the terminal velocity was measured, data were gathered in the middle of the tube away from the ends. Tanner¹² has shown that end effects start to become negligible at a distance of one tube radius from the end; thus all measurements were made in zones at least one tube diameter from the end plates. Since the tubes were easily invertible the fall time of any sphere could be repeated as often as desired. Thus the terminal velocities were obtained as averages of many trials. Only average velocities whose standard deviation was less than 0.1 per cent of the mean were regarded as acceptable.

Since the speed of the particle depends upon the radial eccentricity within the tube, eq. (8), provision was made to measure the radial position at the midpoint of the trajectory. A cathetometer placed in a horizontal position was used to obtain the distance, b , from the center of the sphere to the axis of the tube. The data were corrected for the optical distortion of the viscometer walls with the result that the true radial position was measured to within 0.01 cm.

3.3 Spheres

Spheres of nylon, aluminum oxide, stainless steel and carbide were selected to provide as wide a range of effective shear stress, τ , as practicable. Through this selection of material densities and by variation

of the diameter it was possible to obtain an experimental range of τ from 9 to 735 dynes/cm².

The properties of the spheres were determined by both direct and indirect methods. The carbide, steel and large ruby spheres had accurate size tolerances, and their masses were measured individually. The manufacturer's tolerances for the small ruby spheres were as large as 1.0 per cent, so their properties were checked by dropping them in two Newtonian fluids of known viscosity: Silicone Oil and a Cannon Instrument Company (CIC) standard oil.

The use of plastic spheres has been avoided by other investigators on the grounds that their sphericity is poor. However, it can be shown from Brenner's¹³ drag formulae for rough spheres and from the manufacturer's tolerances that the error in Stokes law is only 0.1 per cent in the worst case. The major problem encountered with the nylon spheres was their density variation due to water absorption from the atmosphere. Special treatment was adopted to maintain these spheres in a usable condition. They were dried in a dessicator and then stored in it throughout the experimental period. In their dry state the size of each sphere was measured optically, and their properties were checked from fall data in the silicone oil. After the tests with the PIB solution were completed the properties of the nylon spheres were checked and found to be unchanged.

4. NEWTONIAN TESTS

4.1 Silicone Oil

The silicone oil was used to check the properties of the nylon and small ruby spheres. Its viscosity was determined by dropping three ruby spheres of known properties in the oil and computing the average value according to Faxen's wall correction formula eq. (10). The results gave a mean value for η of 48.56 poises $\pm 0.2\%$. Then the fall velocities of the small ruby spheres were measured, and the viscosity was computed using the nominal size of each sphere. Figure 2 shows an extreme deviation of 2.5 per cent from the 48.56 poises value indicating a significant source of error in the computational quantities. The viscosity was computed as

$$\eta = \frac{2}{9} a^2 g \frac{\Delta\rho}{U} K \left(\frac{a}{R} \right) \left[1 \pm 2 \frac{\delta a}{a} \pm \frac{\delta\Delta\rho}{\Delta\rho} \mp \frac{\delta U}{U} \right] \quad (10)$$

where $K(a/R)$ is the Faxen wall correction

$$K(a/R) = 1 - \frac{a}{R} W(a/R) ,$$

and the terms in the brackets represent the first order error contributions. The quantities $\delta\Delta\rho/\Delta\rho$ and $\delta U/U$ are small compared to the manufacturer's tolerances on $\delta a/a$. Therefore the value of η was fixed at 48.56 poises and eq. (10) was solved for the radius of the sphere. The results differed significantly from the nominal sizes and in some cases were outside the specified tolerances.

In the case of the nylon spheres the radii were well known from optical measurements; however the density difference $\Delta\rho = \rho_s - \rho_f$ was poorly known. Here ρ_s is the sphere density and ρ_f is the fluid

density which was accurately measured. Thus with η known, eq. (10) was solved for the sphere density ρ_s which would be needed in future computations of the non-Newtonian data. Superficially it would appear that the use of the Newtonian test for the measurement of sphere properties rests on the assignment of an absolute value for the viscosity of the test fluid. However, it is easily shown from eq. (10) that the computation of the radius for the spheres with large $\Delta\rho$ or the density for the spheres with small $\Delta\rho$ is independent of the value of η . In effect the test measures the radius of a small sphere relative to that of a large one whose radius can be accurately measured with a micrometer. Likewise for spheres whose $\Delta\rho$ is small the test measures this quantity relative to that of a sphere whose $\Delta\rho$ is large and accurately measurable with a balance and micrometer. It should be noted that the test cannot be used to accurately measure the radius of a sphere with small $\Delta\rho$. This statement is easily proved by examination of the error terms in eq. (10). The justification for the characterization of spheres by this method can be seen in Figures 4 and 5 where excellent continuity and overlap is obtained between data for nylon spheres ($\Delta\rho$ small) and ruby spheres ($\Delta\rho$ large).

4.2 Cannon Instrument Company Oil

The CIC standard viscosity oil had a nominal viscosity of 26.36 poises $\pm 0.5\%$ at 25°C. This oil was used to check the absolute accuracy of the system and to verify the calibration of the small ruby spheres from the silicone oil tests. During the velocity measurements it was found that temperature fluctuations were the main^{*} sources of error because of the strong sensitivity of the viscosity to temperature. The change in fall

speed was measured to be 9.0 per cent per degree centigrade which when combined with the temperature controller's own fluctuations yields an extreme control error of 0.2 per cent. The results of the viscosity calculations are shown in Figure 2 where the average computed value is 26.27 poises. This differs by only 0.34 per cent from the nominal CIC viscosity and therefore indicates that the absolute accuracy of the measurements is very good.

In the computations for the CIC oil's viscosity, the sphere radii determined from the silicone oil tests were used. This is equivalent to writing eq. (10) once for the silicone oil and once for the CIC oil (R constant) and then eliminating the common factor $2a^2gK(a/R)/9$ between them. The expression for the viscosity then becomes

$$\eta_2 = \eta_1 \frac{U_1}{U_2} \frac{\rho_s - \rho_2}{\rho_s - \rho_1} \left[1 \pm \frac{\delta\eta_1}{\eta_1} \pm \frac{\delta U_1}{U_1} \mp \frac{\delta U_2}{U_2} \pm \frac{\rho_1 - \rho_2}{(\rho_s - \rho_1)} \frac{\delta\rho_s}{(\rho_s - \rho_2)} \right] \quad (11)$$

where subscripts 1 and 2 refer to the silicone oil and CIC oil respectively. The brackets enclose the first order estimates of the error contributions of which η_1 , U_1 and U_2 comprise the significant sources of error for the case of the ruby spheres. The error from ρ_s has been reduced to negligible levels in this case because the fluid densities are close in value to each other ($\rho_1 = 0.9677$, $\rho_2 = 0.7762$ and $\rho_s = 3.994$ gm/cc) causing the coefficient $(\rho_1 - \rho_2)/(\rho_s - \rho_1)$ to be small. The overall effect of eq. (11) is to greatly reduce the scatter in the viscosity as is seen by a comparison of the two sets of data in Figure 2. The silicone oil viscosity was computed without correction for the sphere sizes; whereas the CIC oil viscosity was calculated according to eq. (11) and shows significantly smaller scatter. Much of the scatter which does appear in the CIC oil data may be attributed to temperature fluctuations during the measurements.

5. NON NEWTONIAN TESTS

5.1 Fall Data

All the non-Newtonian studies were made in a solution consisting of 5 per cent PIB and 95 per cent cetane by weight. The PIB (Vistanex MM L-140) had a viscosity average molecular weight of 117,000 to 135,000. During the investigation a trend was noticed whereby the velocity of small ruby and steel spheres drifted by measurable amounts while they became acclimated to the fluid. The trend was small and could not always be detected, but the speed always decreased from the initial value taken immediately after putting the clean dry sphere into the viscometer. If a few hours were allowed to pass or the particle was left in the tube over night, a steady speed would be reached which ranged (in the most obvious cases) from 0.4 to 1.0 per cent below the initial value. In practice it was not possible to wait for the sphere to reach equilibrium within the tube before recording data. Thus the spheres were stored in a small sample of the PIB solution so as to be in equilibrium before being placed in the viscometer. No drifting was observed after this procedure was adopted. It is not possible to give a precise explanation of the drift in the fall times, but it appears to be an effect associated with exposure of fluid surfaces to evaporation and possibly degradation. In some earlier experiments Wilson¹⁴ had observed the fall of spheres which were introduced through a free surface. The velocities he measured varied greatly with the age of the fluid surface. In the extreme case of a PIB solution exposed to the atmosphere for a few days Wilson noticed that the sphere dragged a "skin" from the free surface into the bulk of the solution. The skin was

observable because its refractive index differed slightly from the bulk value. Even after his fall tubes were covered and surface exposure times were minimized it was not possible to obtain fall data free from drift. The closed fall tubes used in the experiments of this paper were designed to overcome these difficulties. It is noteworthy that the drift in fall times was not observed for the dessicated nylon spheres. In view of the precautions taken to minimize the exposure of the fluid surface to evaporation this suggests that the effect depends also on the nature of the solid surface.

In all there were twenty-four different spheres to be used in the viscometer. Eleven of them, from the smallest nylon to the largest carbide, were selected to be dropped in all four tubes. These data, Table I, comprise the information for the wall effect study. The remainder of the spheres were tested in the 4.445 cm tube in order to cover the entire shear stress range with a maximum number of points, Table II. All of the data in Tables I and II are given as center line velocities whereas the actual measurements were made with some radial eccentricity. The velocities were corrected to the axial values, U , according to eq. (8). This correction was checked experimentally and was found to be highly accurate for slow spheres in the neighborhood of the lower Newtonian regime. The errors in the predicted values of U were less than 0.1 per cent in all cases where b/R was small ($b/R \leq 0.1$). For b/R between 0.1 and 0.5 the error in U had an upper limit of about 0.2 per cent for the large steel and carbide spheres. These heavier spheres lie outside the limits of the theory so that the center line correction terms themselves may be as much as 100 per cent in error; but since the correction is a small

portion of the total velocity, the accuracy of U is not diminished significantly.

5.2 Comparison with Theory

The wall effect data, Table I, provides the center line velocities for eleven spheres in four tubes. According to the third order theory, eq. (5), a plot of U versus $W(a/R)/R$ provides $U_{\infty}(F)$ as the intercept, and μ_0 is found from the slope according to the relation

$$\mu_0 = -a^2 \tau / (dU/dG) + 0(\tau^3/R^2) \quad (12)$$

where $G(a,R) = W(a/R)/R$ (see Figure 3). These results should be valid only when τ is small and/or R is large. An inspection shows that deviations exist between the theory and experiment. The first three spheres in Table I have small effective shear stresses so that their predictions for μ_0 via eq. (12) are in good agreement; keep in mind here the fact that the slope is a second order quantity which cannot be measured as accurately as the velocity. Their values of $115.6 \pm 1.9\%$, $114.8 \pm 0.4\%$ and $117.2 \pm 3.8\%$ have overlapping error bounds based upon a 98 per cent confidence limit and yield an average zero shear viscosity of 115.9 poises. Deviations in the prediction of μ_0 begin to appear as one proceeds down the table in the direction of increasing shear stress τ . Here μ_0 decreases monotonically from 115.9 poises with increasing τ . From these results it may be concluded that eq. (5), based upon μ_0 , is strictly valid only over a small range of τ near $\tau = 0$.

A second point of interest is the accuracy of the Newtonian geometry

factor $G(a,R)$. As long as the U versus $G(a,R)$ curve remains a straight line, this factor may be considered an accurate functional representation of the wall's geometrical influence. The data in Table I show a straight line relationship for the first six spheres of which the 0.47625 cm nylon and 0.15875 cm steel spheres are plotted in Figure 3. The last five spheres cover increasing shear stress and being to demonstrate a departure from the linear relationship. The 0.47625 cm carbide sphere, which has the greatest curvature, is shown in Figure 3. Although the first six spheres follow the straight line relation suggested by eq. (5) values of μ_0 calculated from the slope are in agreement with the intercept of Figure 5 only for the smallest values of τ .

Two methods are now available which predict the velocity $U_\infty(F)$ which the sphere would exhibit in an infinite body of fluid. Either eq. (5) may be applied directly using the best estimate for μ_0 or the wall effect data, U versus $G(a,R)$, can be extrapolated to the infinite tube limit. At large shear rates it is already known that eq. (5) will underestimate U_∞ since μ_0 overestimates the effect of viscosity. On the other hand, a linear extrapolation of U versus $G(a,R)$ will overestimate U_∞ due to the curvature of the data. But one important feature is how well these two techniques compare to each other. Table I lists the results for U_∞ by both methods, and it is apparent that agreement is very good over the entire experimental range. At small τ there is virtually no difference between the two values while the worst case, the 0.47625 cm carbide sphere, shows a discrepancy of only 0.8 per cent. Thus there is little practical difference in the results although the method of extrapolation requires the tedious gathering of data in multiple tube sizes.

Once the value of U_{∞} is known for each sphere the apparent viscosity μ can be computed from

$$\mu = F/6\pi aU_{\infty} . \quad (13)$$

Tables I and II list values of μ and τ for each sphere tested. According to the third order theory, eq. (3), $1/\mu$, the apparent fluidity, should be linear in τ^2 for small shear stress; however Figure 4, which gives both $1/\mu$ versus τ and $1/\mu$ versus τ^2 , shows that it is proportional to τ near zero. Although this result disagrees with the theory, it does agree with Turian⁶ who also found $\log\mu$ to be linear in τ and with Peterlin¹⁵ who quotes many experimentalists as finding viscosity proportional to shear rate at low shear rates. A plot of $\log\mu$ versus τ , similar to Turian's, is given in Figure 5. This curve is remarkably linear for τ up to about 240 dynes/cm². A least square fit of a straight line through this region predicts a zero shear viscosity (or intercept) of 116.2 poises \pm 0.1% (based on a 98 per cent confidence limit), and a check of the maximum deviation from the straight line yields a value of 0.03%. This prediction for μ_0 is in very good agreement with the value obtained from the wall effect data for the spheres with the smallest values of τ .

CONCLUSION

The terminal velocity experiments described in this paper were carried out to verify the predictions of the theory of Rivlin-Ericksen fluids for both wall-effects as expressed by eq. (5) and for the asymptotic approach to zero-shear rate conditions as expressed by eq. (3). The study of these effects demands measurements whose precision is high compared to

that attainable in most viscometers based on viscometric flows. For this reason the sealed fall tubes described above were employed to obtain a high degree of stability of the fluid properties over long periods of time. In addition, the invertibility of these tubes permitted the repetition of any fall so that the reproducibility of a terminal velocity could be conveniently checked. The spheres themselves had to be given special treatment to insure reproducible fall speeds. The nylon spheres were dessicated to maintain constant density and size, and the ruby, steel, and carbide spheres were stored in the PIB solution before use in order to avoid the drift in fall velocity observed when a dry sphere is first introduced into the solution. Finally, in order to calculate apparent viscosities of accuracy comparable to that of the terminal velocities it was necessary to determine the properties of some of the spheres in tests with fluids which are known to be Newtonian. This was necessary because their sizes and weights could not be determined with sufficient accuracy with conventional methods. The justification of this sphere calibration can be seen in Figure 4 which shows the excellent overlap and continuity between the nylon and ruby points.

Wall effects for data taken in tubes can be computed very well with eq. (5) provided the limitations suggested by the error term are recognized. Thus relatively large spheres can be used if their densities are close to the fluid density so that the net force is small. As the solid-fluid density difference increases it is necessary to reduce the sphere size or increase the tube diameter until the wall correction is a small part (about 10 per cent) of the total velocity. In most experimental designs it is desirable to minimize the volume of fluid required, and this inevitably means the wall correction tends to become large. Until the non-Newtonian

terms in eq. (5) have been calculated from an adequate theory it is recommended that terminal velocities should be measured in tubes of at least two different diameters. The degree of agreement between the U_{∞} values calculated from eq. (5) is then a measure of the importance of the missing terms.

The most interesting result of these experiments is the linear departure from μ_0 of the apparent viscosity μ in terms of τ as shown in Figure 4. This is in direct contradiction to the quadratic departure predicted by the Rivlin-Ericksen theory. These experiments also confirm to a very high degree of precision Turian's⁶ earlier finding of an exponential range which extends well beyond the linear region. Turian's falling sphere experiments were carried out with several polymers at several concentrations and temperatures, and in each case an exponential range was found. The experiments described here while they include data on only one solution are considerably more precise than those of Turian.

While the apparent viscosity, eq. (13), based on Stokes law is not directly comparable to the viscosity function of the viscometric flows, it is worth noting that the latter generally exhibits exponential behavior at low shear stresses (see Peterlin¹⁵). The theories referred to above are all based upon continuum concepts. However, the theories of the viscosity function which are based upon molecular ideas also predict a quadratic law of departure from the zero-shear rate viscosity (see Peterlin¹⁵).

Any new calculations for flow past a sphere must be based on theories in which the viscosity function can depend on odd powers of the shear rate. Such calculations should include the effect of boundaries in order that experimental terminal velocity measurements can be interpreted. The wall

effect is used not only to calculate U_{∞} values but also provides an independent although less accurate method for the calculation of μ_0 . This self-consistency check of μ_0 provided by the wall effect makes the falling sphere experiment particularly well suited to the study of the approach to the zero-shear rate regime.

ACKNOWLEDGMENTS

The authors gratefully acknowledge the assistance of Dr. Robert Marvin of the National Bureau of Standards in the evaluation of the properties of the standard viscosity oil which was kindly supplied by Dr. Robert Manning of the Cannon Instrument Company. The polyisobutylene (Vistanex) and its stabilizing agent were supplied by the Enjay Chemical Company. Financial support was provided by the National Aeronautics and Space Administration ~~under grant NGL-40~~ and in the form of a NASA Traineeship for D.A.C.

REFERENCES

- ¹F. M. Leslie, *Quart. J. Mech. Appl. Math.* 14, 36 (1961).
- ²H. Giesekus, *Rheologica Acta* 3, 59 (1963).
- ³B. Caswell and W. H. Schwarz, *J. Fluid Mech.* 13, 417 (1962).
- ⁴B. Caswell, *The Effect of Finite Boundaries on the Motion of Particles in Non-Newtonian Fluids*, *Chem. Eng. Sci.*, in press.
- ⁵B. Caswell, *The Stability of Particle Motion near a Wall in Newtonian and Non-Newtonian Fluids*, *Chem. Eng. Sci.*, under review.
- ⁶R. M. Turian, PhD Dissertation, Dept. of Chemical Engineering, University of Wisconsin, Madison, Wisconsin (1964).
- ⁷H. Brenner, *J. Fluid Mech.* 18, 144 (1964).
- ⁸J. Happel and H. Brenner, *Low Reynolds Number Hydrodynamics* (Prentice-Hall, Englewood Cliffs, N. J., 1965).
- ⁹R. I. Tanner, *Chem. Eng. Sci.* 19, 349 (1964).
- ¹⁰E. Ashare, *Trans. Soc. Rheol.* 12, 535 (1968).
- ¹¹H. Brenner and J. Happel, *J. Fluid Mech.* 4, 195 (1958).
- ¹²R. I. Tanner, *J. Fluid Mech.* 17, Part 2, 161 (1963).
- ¹³H. Brenner, *Chem. Eng. Sci.* 19, 519 (1964).
- ¹⁴D. S. Wilson, M.S. Dissertation, Dept. of Chemical Engineering, University of California, Davis, California (1965).
- ¹⁵A. Peterlin, *Advances in Macromolecular Chemistry*, W. M. Pasika, Ed. (Academic Press, New York, 1968), Vol. 1.

TABLE I

Wall Effect Data for the PIB Solution

Nominal Sphere Diameter ^a cm	Centerline Velocity U cm/sec				Tube #4	U _∞ ^b cm/sec	μ ₀ ^c Poises	U _∞ ^d cm/sec	μ ^e Poises	F/6πa ² dyn/cm ²
	Tube #1	Tube #2	Tube #3	Tube #4						
0.23813 N	0.007491	0.008027	0.008529	0.008973	0.009592	115.6	0.009595	115.1	9.349	
0.47625 N	0.02241	0.02661	0.03046	0.03401	0.03908	114.8	0.03904	114.3	18.83	
0.07938 R	0.009049	0.009253	0.009400	0.009558	0.009762	117.2	0.009768	113.4	27.86	
0.15875 R	0.03406	0.03562	0.03690	0.03816	0.03984	113.7	0.03983	110.6	55.58	
0.23813 R	0.07252	0.07779	0.08214	0.08631	0.09204	113.6	0.09195	108.1	83.46	
0.15875 S	0.07792	0.08131	0.08411	0.08664	0.09040	113.4	0.09023	104.8	119.1	
0.47625 R	0.2391	0.2822	0.3176	0.3507	0.3980	110.1	0.3957	100.5	166.9	
0.3175 S	0.2974	0.3257	0.3479	0.3694	0.3999	108.5	0.3978	94.46	236.7	
0.47625 S	0.6328	0.7425	0.8189	0.8916	0.9953	107.0	0.9874	85.75	355.6	
0.3175 C	0.7951	0.8621	0.9120	0.9579	1.0227	105.1	1.0167	76.49	489.9	
0.47625 C	1.903	2.173	2.386	2.541	2.762	103.9	2.739	63.93	735.4	

^aC-carbide; N-nylon; R-ruby; S-steel.

^bU_∞ taken as the intercept of U versus G(a,R).

^cμ₀ computed via eq. (12).

^dU_∞ computed via eq. (5) with μ₀ = 116P and U from tube #4.

^eμ computed via eq. (13) using U_∞^d.

TABLE II

Fall Data for the PIB Solution in Tube #3

Nominal Sphere Diameter ^a cm		U cm/sec	U _∞ ^b cm/sec	μ Poises	F/6πa ² dyn/cm ²
0.3175	N	0.01466	0.01722	115.1	12.50
0.039688	R	0.002381	0.002426	114.7	13.96
0.39628	N	0.02232	0.02737	114.5	15.78
0.55563	N	0.03984	0.05343	114.2	22.07
0.07	R	0.007396	0.007646	113.5	24.67
0.08	R	0.009523	0.009889	113.2	28.01
0.10	R	0.01481	0.01553	112.7	35.03
0.15	R	0.03318	0.03561	111.1	52.65
0.18	R	0.04771	0.05191	110.0	63.26
0.3175	R	0.1444	0.1672	105.7	111.35
0.39688	R	0.2234	0.2679	103.1	139.19
0.23813	S	0.1923	0.2129	99.34	177.61
0.39688	S	0.5541	0.6483	90.34	295.17

^aC-carbide; N-nylon; R-ruby; S-steel.

^bU_∞ computed via eq. (5) with μ₀ = 116P.

FIGURE CAPTIONS

- Figure 1: Viscometer tube.
- Figure 2: Newtonian viscosity measurements: (\square) silicone oil calibration points $\eta_{ave} = 48.56P$; (\blacksquare) silicone oil test points; (\odot) CIC oil test points.
- Figure 3: Terminal center line velocity versus tube influence factor $G(a,R)$.
- Figure 4: Apparent fluidity versus shear stress in the low shear range. (\blacktriangle) nylon data against τ ; (\triangle) ruby data against τ ; (\odot) nylon data against τ^2 ; (\circ) ruby data against τ^2 . Solid curve from the straight line fit of $\log \mu$ versus τ (see Figure 5).
- Figure 5: Log of the apparent viscosity versus shear stress: (∇) carbide; (\odot) nylon; (\blacktriangle) ruby; (\blacksquare) steel.

gb
4/16/70

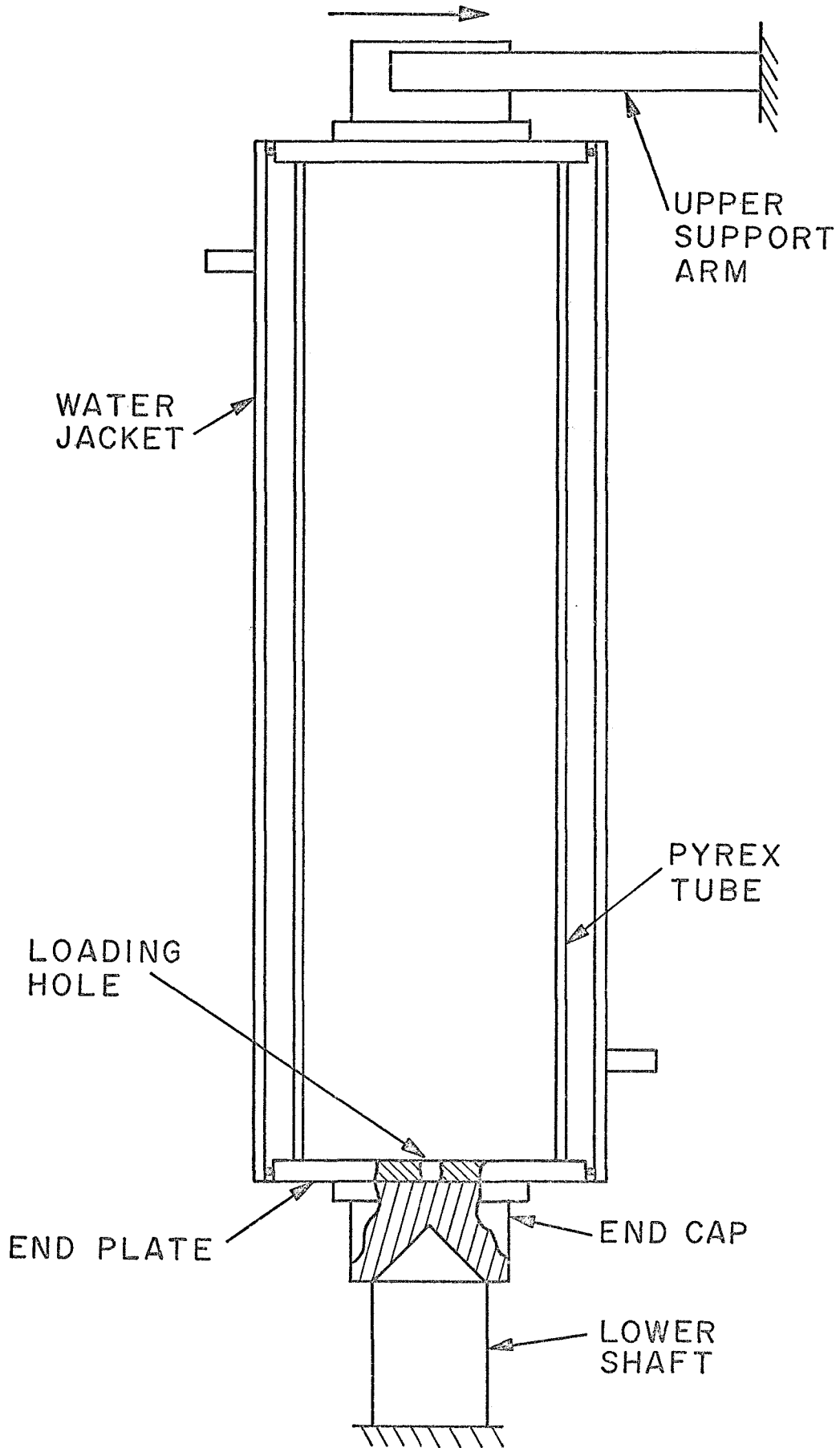


FIGURE 1

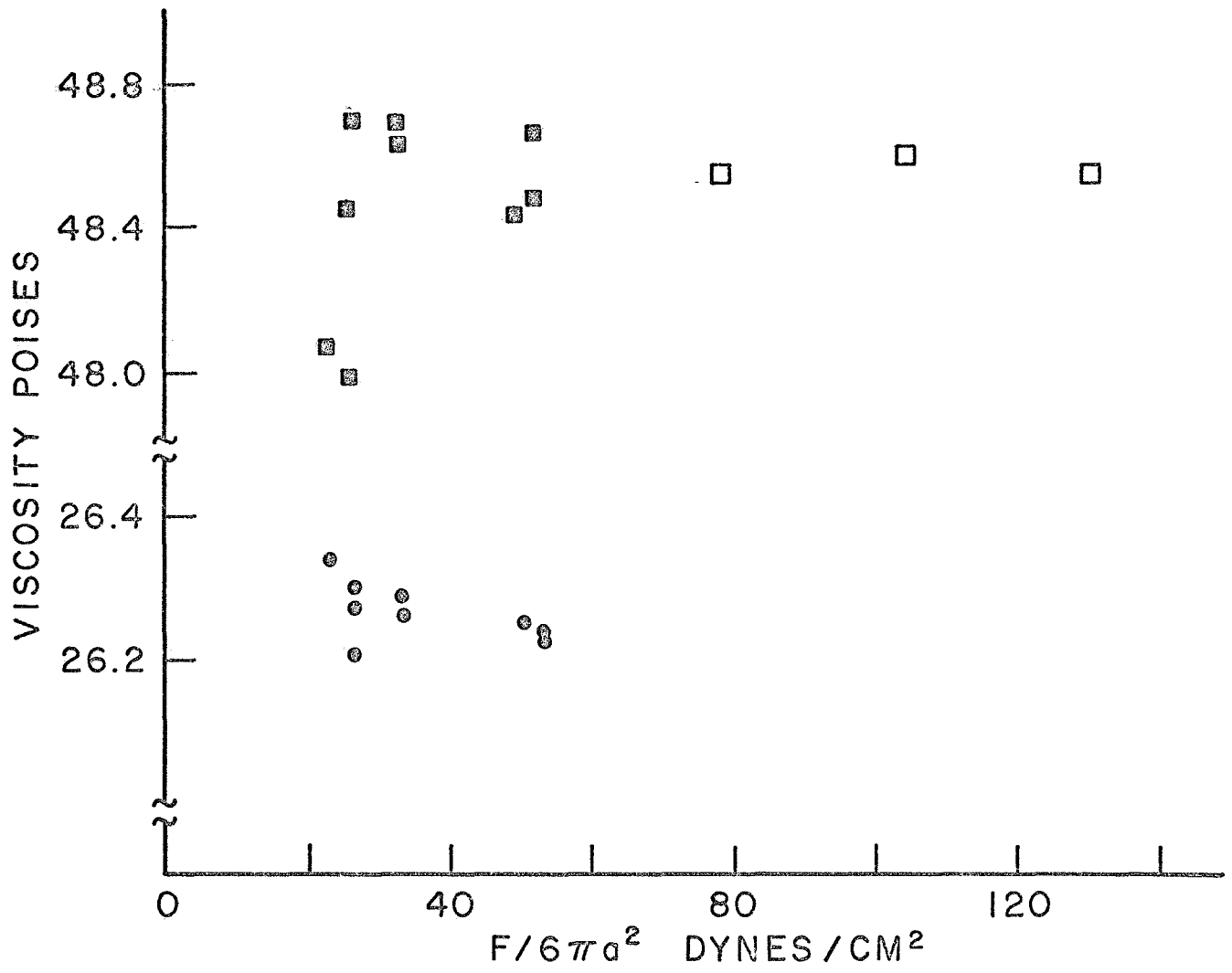


FIGURE 2

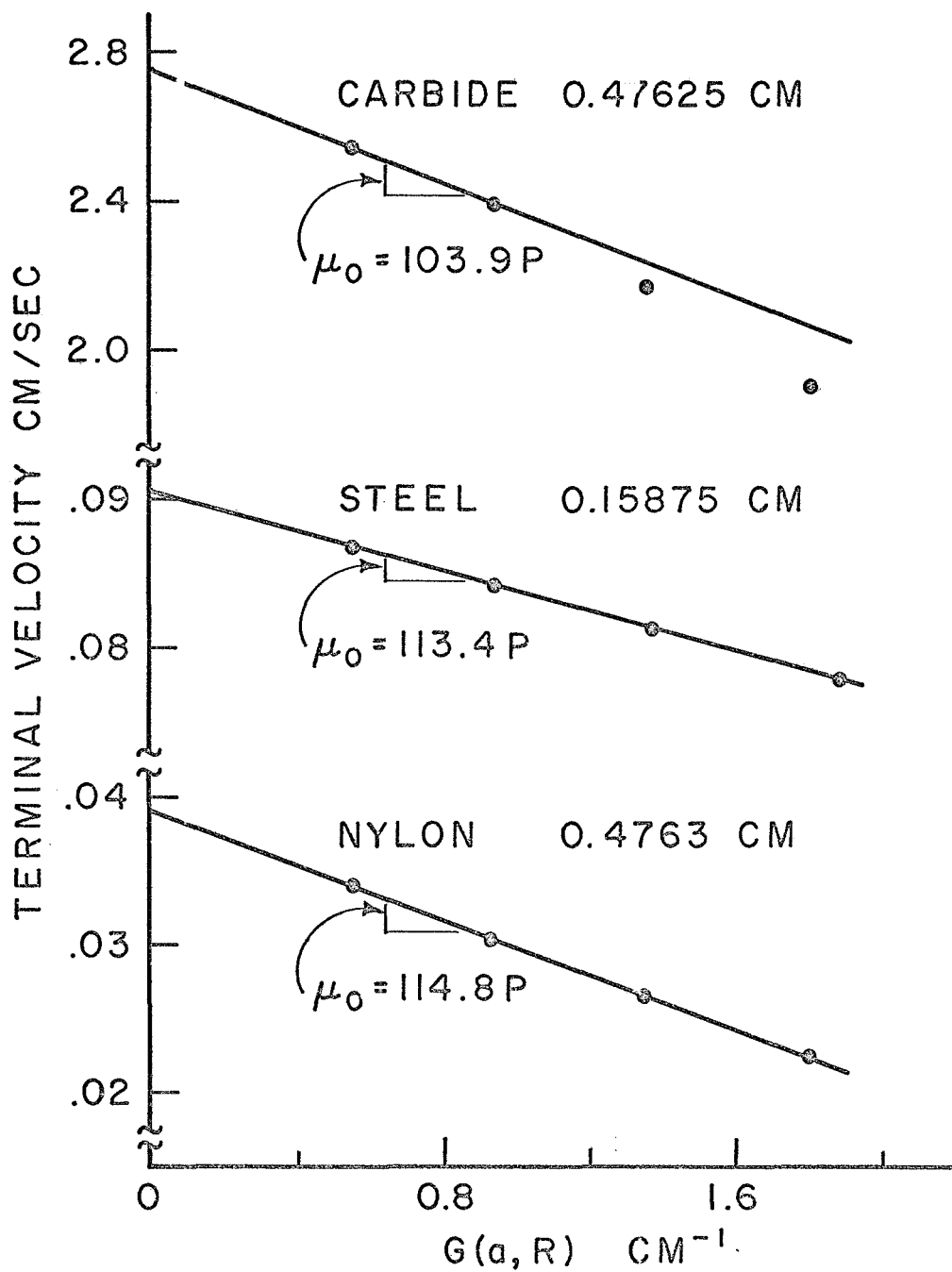


FIGURE 3

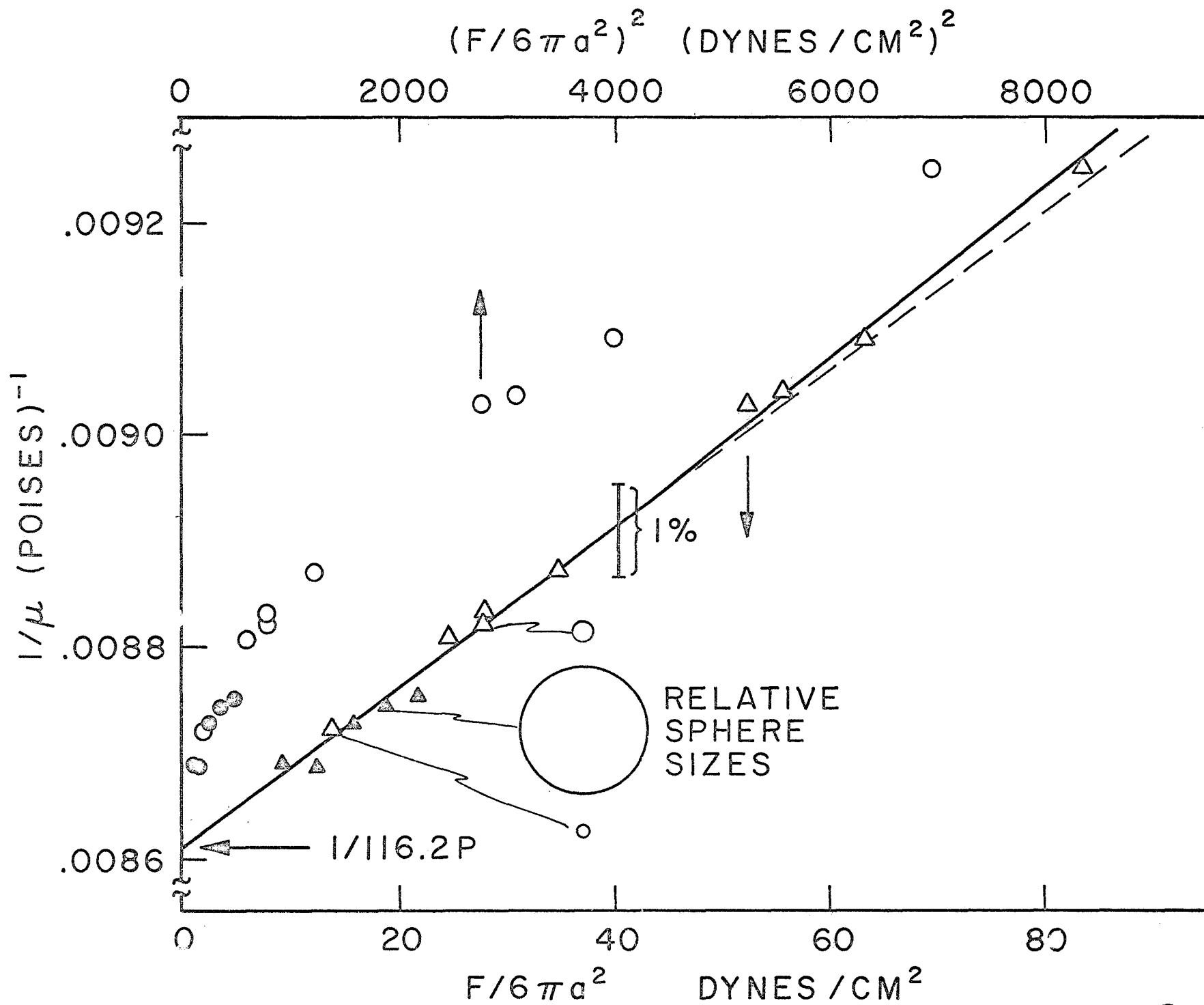


FIGURE 4

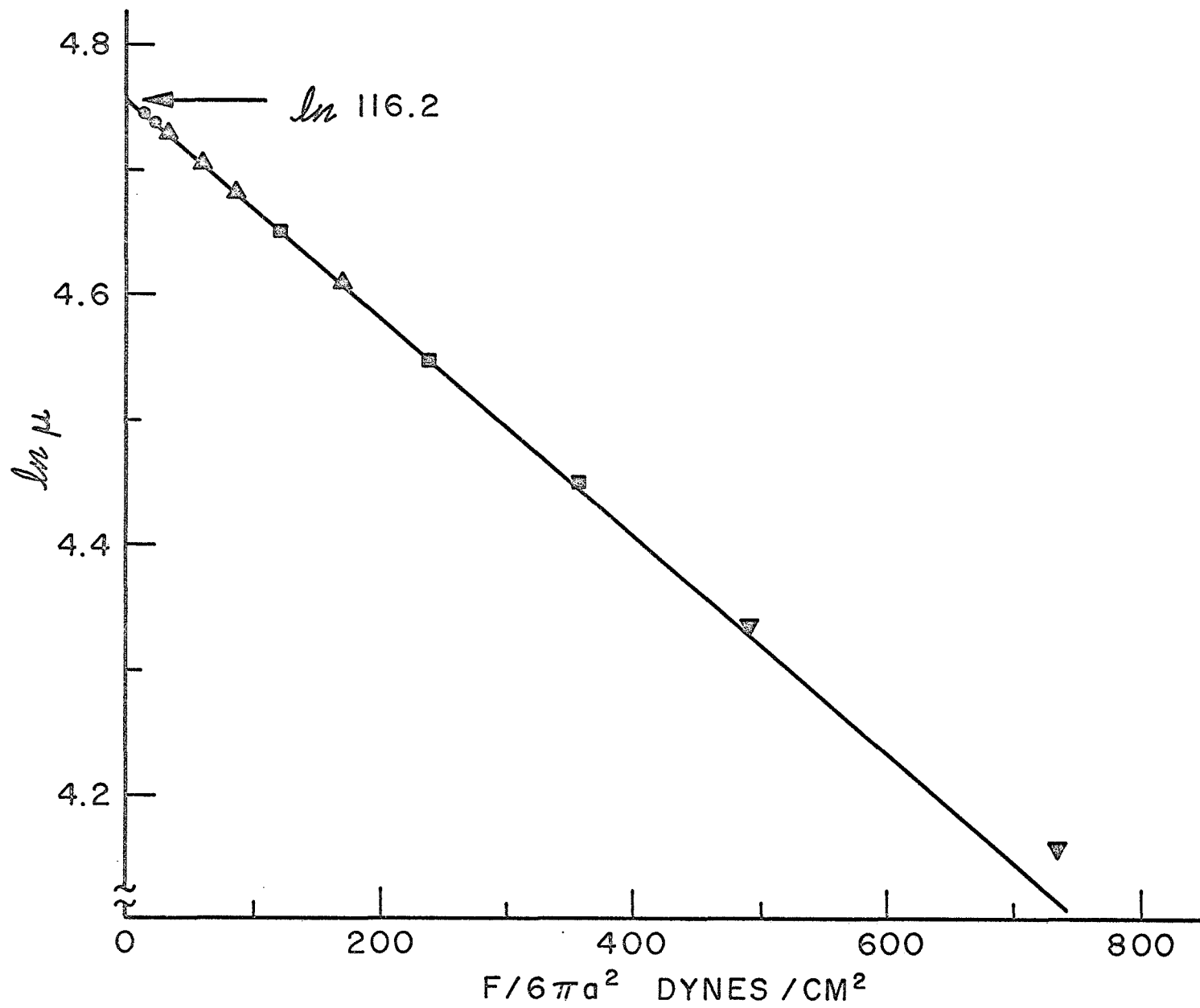


FIGURE 5